Modeling the Energy-dependent Gamma-ray Light Curves of the Vela Pulsar

Monica Barnard[1], **Christo Venter**[1], **Alice K. Harding**[2] **and Constantinos Kalapotharakos**[2,3,4]

[1]Centre for Space Research, North-West University, Potchefstroom 2520, South Africa
[2]Astrophysics Science Division, NASA Goddard Space Flight Center, Greenbelt, MD 20771, USA
[3]Universities Space Research Association (USRA), Columbia, MD 21046, USA
[4]University of Maryland, College Park (UMDCP/CRESST), College Park, MD 20742, USA

monicabarnard77@gmail.com, christo.venter7@gmail.com, ahardingx@yahoo.com, c.kalapotharakos@gmail.com

Abstract

Detection of the Vela pulsar up to ∼100 GeV by H.E.S.S. and the Fermi Large Area Telescope (LAT) provides evidence for a curved spectrum. We interpret this spectrum to be the result of curvature radiation by primary particles in the pulsar magnetosphere and current sheet. We present energy-dependent light curves with good resolution for several different parameters using a full emission code, assuming a force-free magnetic field and uniform emissivity. We include a refined calculation of the curvature radius of particle trajectories, which has an influence on the transport, predicted light curves, and spectra. We find that the curvature radii of trajectories associated with the second gamma-ray light curve peak are relatively larger than those associated with the first, leading to larger cutoffs and explaining the disappearance of the first peak at higher energy. We fit model light curves to the radio and energy-dependent gamma-ray data. To address the larger-than-observed prediction of the radio-to-gamma phase lag, we will in future focus on a more self-consistent force-free inside and dissipative outside (FIDO) model. Multi-band energy-dependent light curve modeling thus presents an important tool to constrain models of pulsar emission and magnetospheric structure.

Introduction

Over the past decade three pulsars have been detected by ground-based Cherenkov telescopes in the very-high-energy (VHE, > 100 GeV) band. MAGIC has detected pulsed emission from the Crab pulsar up to 1.5 TeV [1] and H.E.S.S. detected the Vela pulsar above 3 TeV [2]. Lastly, MAGIC has recently detected pulsed emission from the Geminga pulsar above tens of GeV. Pulsar light curves exhibit structure that evolves with photon energy E_γ. This is also seen in data from ground-based Cherenkov telescopes. Notably, as E_γ is increased, the main peaks of Crab and Vela seem to remain at the same normalized phase, the intensity ratio of the first to second peak decreases, and the peak widths decrease [3]. By constructing detailed physical models, one may hope to disentangle the underlying electrodynamics and acceleration processes occurring in the magnetosphere.

Model Description

We use a full emission code that assumes a 3D force-free B-field structure and constant E-field [4]. The force-free solution formally assumes an infinite plasma conductivity, so that the E-field is fully screened and serves as a good approximation to the geometry of field lines implied by the dissipative models that require a high conductivity in order to match observed γ-ray light curves [5, 6, 7]. The primary particles (leptons) are injected at the stellar surface with a low initial speed and are accelerated by a constant E-field in a slot gap (SG) scenario near the last open field lines. The gap reaches beyond the light cylinder radius $R_{\rm LC} = c/\Omega$ (where the corotation speed equals the speed of light c with Ω the angular speed) up to $r = 2R_{\rm LC}$. Some of the primaries accelerated near the polar cap radiate curvature radiation (CR) and some of these γ-ray photons are converted into pairs causing a pair cascade.

Refinements of curvature radius

As a first approach we refined the first-order calculation of the curvature radius $\rho_{\rm c}$ along the particle trajectory, assuming that all particles follow the same trajectory, independent of their energy. To calculate the electron's trajectory as well as its $\rho_{\rm c}$ we used a fixed small step length along the B-field line. The first derivative (direction) is equivalent to the normalized B-field components as a function of the cumulative arclength s. First we step along a particular field line. Second, we smooth the positions and their directions using s as the independent variable. Third, we match the unsmoothed and smoothed positions and their directions of the particle trajectory at particular s values to get rid of unwanted "tails" at low and high altitudes, introduced by the use of a kernel density estimator (KDE) smoothing procedure. Fourth, we use a second-order method involving a Lagrange polynomial to obtain the second-order derivatives of the directions along the trajectory as function of s. Lastly, we match $\rho_{\rm c}$ calculated using smoothed and unsmoothed directions to get rid of "tails" at low and high altitude. We then interpolate $\rho_{\rm c}$ in our particle transport calculations to accommodate the variable step length approach.

Both the particle transport equation [4] and the spectral energy cutoff ([8]; in the CR reaction limit) scale with $\rho_{\rm c}$ as seen in Equation (1) and (2). In Equation (1) only the first and third terms are contributing to the transport, since we consider CR from primaries only. Peak 2 with the larger $\rho_{\rm c}$ should have a larger $E_{\gamma,\rm cutoff}$ (see Figure 3; Barnard et al. (2018), in prep.).

Particle transport equation

$$\frac{d\gamma}{dt} = \frac{eE_\parallel}{mc} - \frac{2e^4}{3m^3c^5}B^2p_\perp^2 - \frac{2e^2\gamma^4}{3\rho_c^2} + \left(\frac{d\gamma}{dt}\right)^{\rm abs} - \left(\frac{d\gamma}{dt}\right)^{\rm SSC} \quad (1)$$

Spectral energy cutoff

$$E_{\gamma,\rm cutoff} \sim 4E_{\parallel,4}^{3/4}\rho_{c,8}^{1/2} \quad (2)$$

Results

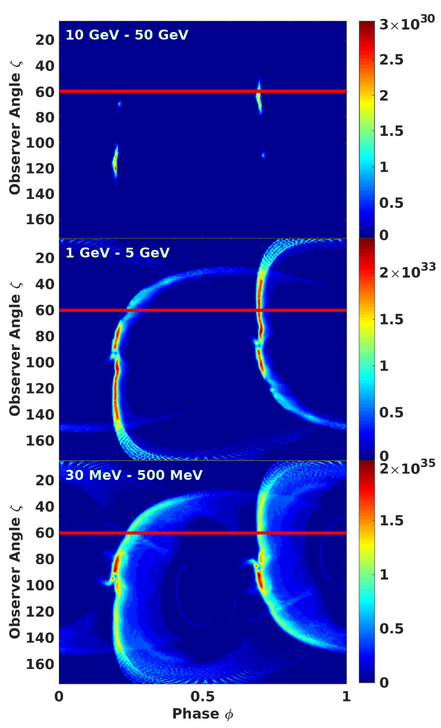

Figure 1: *Force-free phase plots for $\alpha = 75°$, $\zeta = 60°$ (red line) and for three different energy-bands in the range 30 MeV $< E_\gamma < 50$ GeV (increasing from bottom to top as indicated by the legend).*

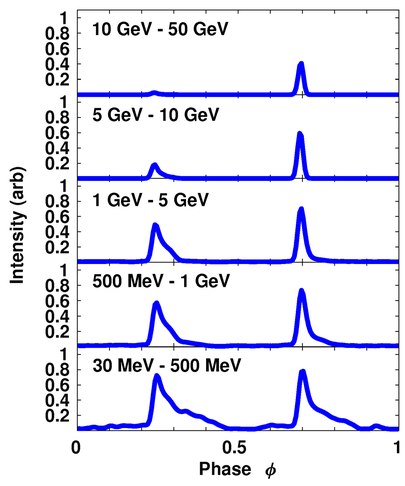

Figure 2: *Force-free energy-dependent light curves (with the top, middle and bottom panels corresponding to Figure 1) for $\alpha = 75°$, $\zeta = 60°$, and 30 MeV $< E_\gamma < 50$ GeV (increasing from bottom to top as indicated by the legend).*

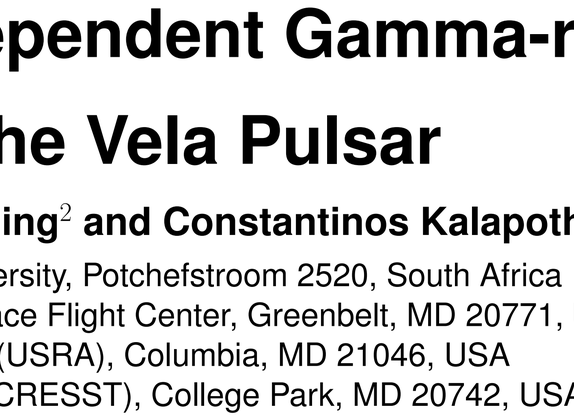

Figure 3: *The ratio between $\rho_{\rm c}$ (as a function of $s/R_{\rm LC}$) for the second and first peak remains roughly constant inside the light cylinder and then abruptly increases at and beyond the light cylinder (i.e., in the current sheet).*

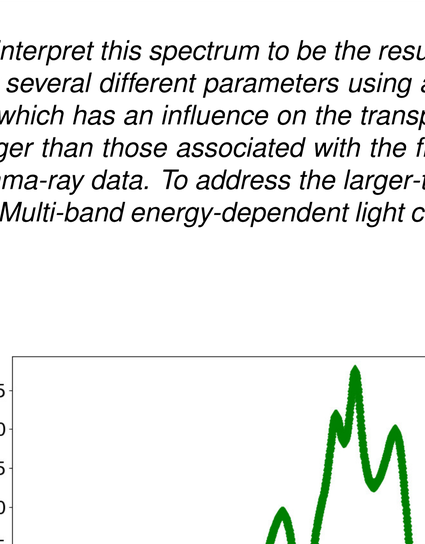

Figure 4: *Fitting the radio and energy-dependent γ-ray model light curves (blue solid line) for $\alpha = 75°$ and $\zeta = 63°$ [9], to the radio, Fermi-LAT ($0.3 < E_\gamma < 1$ GeV [10]; compare to Figure 2), and H.E.S.S. II (for the model $E_\gamma > 40$ GeV) [11] data (black solid line).*

Conclusions

Modelling of E_γ-dependent pulsar light curves as well as their spectra is vital to disentangle the effects of acceleration, emission, beaming, and B-field geometry. We used a 3D emission model assuming CR from primary particles in an SG reaching $2R_{\rm LC}$ to study the evolution of the predicted light curves in different E_γ-bands. We find that emission from beyond $R_{\rm LC}$ (in the current sheet) constitutes an important contribution to the light curve structure. We also observe that the predicted ratio of the first to second peak intensity decreases with E_γ. In our model the second peak becomes narrower with increasing E_γ, and its position in phase remains steady with E_γ, similar to what has been observed for the Crab and Vela pulsars.

The refinement of $\rho_{\rm c}$ changed the phase plots and light curves slightly (see Figure 1 and 2). The $\rho_{\rm c}$ is greater for peak 2 than peak 1, leading to a greater $E_{\gamma,\rm cutoff}$ for peak 2. This may explain phenomena seen by *Fermi* and H.E.S.S. II. Continued spectral, light curve and now polarisation modelling [12, 13], confronted by quality measurements, may provide the key to discriminate between different models.

Force-free sky maps with assumed uniform emissivity in azimuth give too large a radio phase lag (see Figure 4). In future we will look at more advanced (self-consistent) models, i.e., FIDO (see, e.g., [7, 14]) or particle-in-cell (see, e.g., [15, 16, 12, 17, 18, 19, 20]) in order to find a better radio and γ-ray fit. These models will predict a smaller radio to γ phase lag that are consistent with the *Fermi* data. The sensitivity of H.E.S.S. II and the upcoming CTA will assist us in finding more pulsars of these new class of VHE pulsars.

This work is based on the research supported wholly / in part by the National Research Foundation of South Africa (NRF; Grant Numbers 99072). The Grantholder acknowledges that opinions, findings and conclusions or recommendations expressed in any publication generated by the NRF supported research is that of the author(s), and that the NRF accepts no liability whatsoever in this regard. A.K.H. acknowledges the support from the NASA Astrophysics Theory Program. C.V. and A.K.H. acknowledge support from the *Fermi* Guest Investigator Program.

References

[1] Ansoldi, S. 2016, A&A, 585, A133
[2] de Naurois, M. 2015, 34th ICRC, 34, 21
[3] Aleksić, J. 2012, A&A, 540, A69
[4] Harding, A. K., & Kalapotharakos, C. 2015, ApJ, 811, 63
[5] Kalapotharakos, C., Kazanas, D., Harding, A. K., & Contopoulos, I. 2012, ApJ, 749, 2
[6] Li, J., Spitkovsky, A., & Tchekhovskoy, A. 2012, ApJ, 746, 60
[7] Kalapotharakos, C., Harding, A. K., & Kazanas, D. 2014, ApJ, 793, 97
[8] Venter, C., & De Jager, O. C. 2010, ApJ, 725, 1903
[9] Ng, C.-Y., & Romani, R. W. 2008, ApJ, 673, 411
[10] Abdo, A. A., *et al.* 2010, ApJ, 713, 154
[11] Abdalla, H., *et al.* 2018, *accepted for publication in A&A*
[12] Cerutti, B., Philippov, A. A., & Spitkovsky, A. 2016, MNRAS, 457, 2401
[13] Harding, A. K., & Kalapotharakos, C. 2017, ApJ, 840, 73
[14] Kalapotharakos, C., Harding, A. K., Kazanas, D., & Brambilla, G. 2017, ApJ, 842, 80
[15] Belyaev, M. A. 2015, NewA, 36, 37
[16] Cerutti, B., *et al.* 2015, MNRAS, 448, 606
[17] Chen, A. Y., & Beloborodov, A. M. 2014, ApJL, 795, L22
[18] Kalapotharakos, C., *et al.* 2018, ApJ, 857, 44
[19] Philippov, A. A., & Spitkovsky, A. 2014, ApJL, 785, L33
[20] Philippov, A. A., Spitkovsky, A., & Cerutti, B. 2015, ApJL, 801, L19